J.Serb.Chem.Soc. 66(11–12)785–797(2001) UDC 66.087.3:546.262.3–31+546.92
JSCS –2903 *Original scientific paper*

Electrochemical oxidation of carbon monoxide: from platinum single crystals to low temperature fuel cells catalysts. Part I: Carbon monoxide oxidation onto low index platinum single crystals*

BRANIMIR N. GRGUR[1**#], NENAD M. MARKOVIĆ[2], CHRISS A. LUCAS[3] and PHILIP N. ROSS JR[2]

[1]Faculty of Technology and Metallurgy, University of Belgrade, Karnegijeva 4, YU-11001 Belgrade, Yugoslavia, [2]Lawrence Berkeley National Laboratory, 1 Cyclotron Road, MS 2-100, Berkeley, CA 94720, USA, and [3]Oliver Lodge Laboratory, Department of Physics, University of Liverpool, Liverpool L69 7ZE, UK

(Received 16 July 2001)

The electrochemical oxidation of carbon monoxide and the interfacial structure of the CO adlayer (CO_{ads}) on platinum low index single crystals, Pt(111), Pt(100) and two reconstruction of Pt(110), were examined using the rotation disk electrode method in combination with the *in situ* surface X-ray diffraction scattering technique. The mechanism of CO oxidation is discussed on the basis of the findings that, depending on the potential, two energetic states of CO_{ads} exist on the platinum surfaces. Thus, at lower potentials, weakly bonded states ($CO_{ads,w}$) and at higher potentials strongly bonded states ($CO_{ads,s}$) are formed. The mechanism of the oxidation of hydrogen-carbon monoxide mixtures is also proposed.

Keywords: platinum single crystals, carbon monoxide, electrooxidation, hydrogen, mechanism.

INTRODUCTION

Low temperature fuel cells based on polymer electrolytes (polymer electrolytes fuel cells, PEFC) are today one of the most promising electrochemical power sources for application in transportation and portable power generation. Hydrogen generated by the steam reforming of methanol, with a typical reformer gas composition ≈75 % H_2, ≈25 % CO_2 and 1–2 % CO, was widely considered as a fuel for the low temperature fuel cells.[1] A major problem in the development of PEFC has been the deactivation of the Pt

* Dedicated to Professor Dragutin M. Dražić on the occasion of his 70th birthday.

** Corresponding author: BNGrgur@elab.tmf.bg.ac.yu.

Serbian Chemical Society active member.

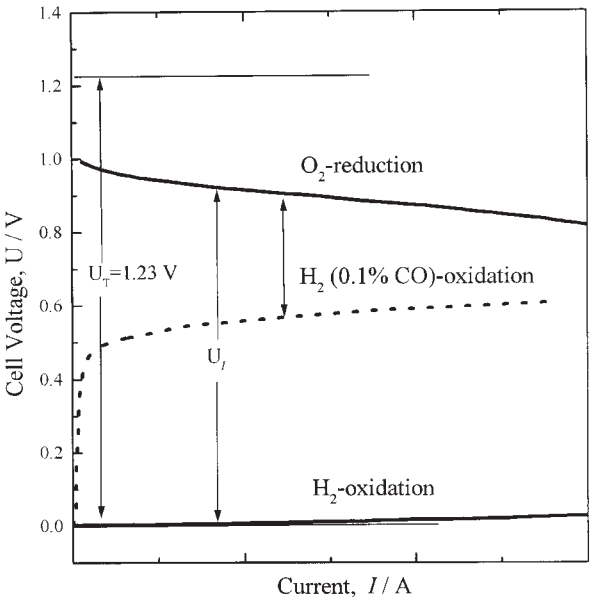

Fig. 1. Voltage–current dependencies of fuel cell reactions.

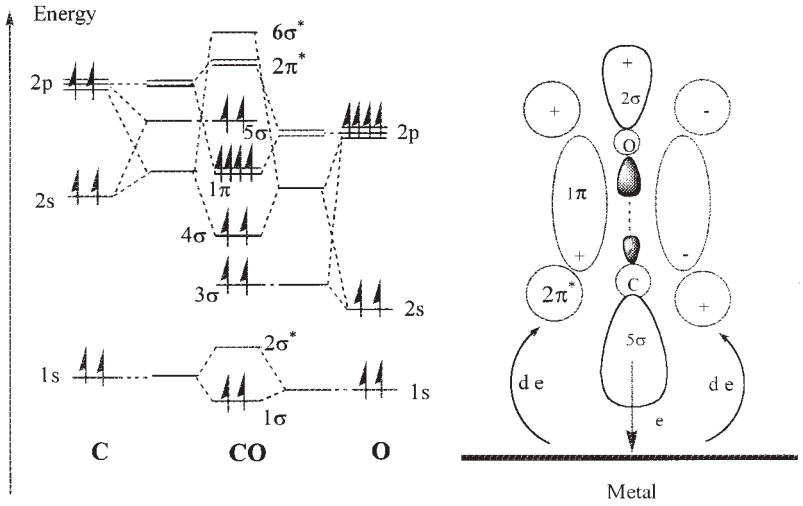

Fig. 2. The energy levels of carbon monoxide molecules and the formation of metal–carbon monoxide bonding.

anode, as the best hydrogen electrooxidation catalyst, by even trace levels, *e.g.,* 5–10 ppm, of carbon monoxide. Without CO in the gas mixtures, the cell voltage, *U*, for the system based on hydrogen oxidation and oxygen reduction on platinum catalysts is between 0.8 and 1 V depending on the output cell current, as shown in Fig. 1. The operating cell voltage is smaller than the theoretical one of 1.23 V, mainly because of the slow oxygen reduction kinetics. In the presence of 0.1 % CO in the hydrogen fuel, dotted line in Fig. 1, the anode voltage loss is 0.5 to 0.6 V, and cell voltage is reduced to only 0.4 to

0.5 V, which is an unacceptable high loss. This is due to strong CO adsorption on the platinum surfaces (CO_{ads}), which leads to the "poisoning" of the active sites for the hydrogen oxidation reaction. Such strong binding has been explained by Blyholder[2] by electron donation from the 5σ carbon monoxide orbital to the metal, and the subsequent transfer of two electrons from the d metal atomic orbitals to the antibonding $2\pi^*$ CO orbital, as shown in Fig. 2. This electron transfer is know as back-donation.

To remove CO_{ads} from the surface it is necessary to generate some oxygenated species that can react with CO_{ads} producing CO_2 and thereby to release some free sites on the Pt surface for the hydrogen oxidation reaction. The mechanism for the oxidative removal of CO_{ads} poison from platinum anodes has been a topic of intense investigation for the past 35 years. The overall reaction for removing CO_{ads} is

$$CO_{ads} + H_2O \rightarrow CO_2 + 2H^+ + 2e^- \quad (1)$$

but the mechanistic details have been elusive. The thermodynamic potential for reaction (1) lies close to 0 V *versus* the reversible hydrogen electrode. Gilman[3] suggested that an adsorbed water molecule attacks an adsorbed carbon monoxide molecule with subsequent and separate deprotonation and electron transfer steps. Some other authors considered that CO_{ads} oxidation proceeds through reaction with OH_{ads}. The oxidation of CO_{ads} by OH_{ads} proceeds as follows

$$CO_{ads} + OH_{ads} \rightarrow CO_2 + H^+ + e^- \quad (2)$$

The hydroxyl group is formed by the dissociative adsorption of a water molecule on the platinum

$$H_2O \rightarrow OH_{ads} + H_{ads} \quad (3)$$

The evidence that OH_{ads} is an active species in reaction (2) comes from the coincidence of the potential for the onset of H_2O oxidation with the potential of CO oxidation. The formation of OH_{ads} on platinum lies between 0.5 to 0.8 V, which is the main reason why platinum oxidizes CO in that potential region. It should be noted that some small CO_{ads} oxidation occur on platinum even at lower potentials, *e.g.,* 0.3 to 0.5 V.[4,5] This oxidation is known as pre-wave oxidation, but there is no practical point of view for that reaction. To shift the CO oxidation to more negative potentials, it is necessary to provide OH at lower potentials. This can be done by means of some other metal, alloyed with platinum, which can generate OH_{ads} at lower potentials on the surface for the oxidation of CO_{ads} on adjacent Pt sites. Such catalysts are known as bi-functional catalysts.[6]

Pt-Ru[7] and Pt-Sn[8] alloy electrodes have been reported to have encouraging catalytic performances in the electrooxidation of H_2/CO mixtures. Unfortunately, even with these catalysts and a low level of CO, ≈100 ppm in the H_2/CO fuel, the voltage losses in a real PEFC are too high, (for PtRu alloy ≈0.4 V at 0.6 A cm^{-2}).[9] This is because CO is adsorbed on the Ru sites as well, blocking these sites for OH nucleation.

The aim of this paper is to summarize some new findings concerning the electrochemical oxidation of CO on pure platinum low-index single crystal electrodes, as a model catalyst, which were used in the development of new platinum molybdenum catalysts.

EXPERIMENTAL

Low index platinum single crystals Pt(*hkl*), Pt(111), Pt(100), Pt(100)–(1×1) and Pt(110)–(1×2) (miscut < 0.2 º) were prepared before each experiment by the flame annealing method. Briefly summarizing, following flame-annealing in a hydrogen flame and subsequent cooling to room temperature in either an argon or hydrogen steam, the single crystal was mounted in the disk position of an insertable rotating disk electrode (RDE) assembly (Pine Instruments).[10] Subsequently, it was transferred into a standard electrochemical cell equipped with a water jacket. CO oxidation was performed in two kind of experiments. In the first type, CO was adsorbed onto Pt(*hkl*) for 5 min at 0.05 V and the solution was then purged with argon for 30 min. This CO oxidation will be referred to as CO_{ads} oxidation. In the second type, the solution was saturated with 100 % CO gas holding the potential of the Pt(*hkl*) at 0.05 V for 5 min and then the CO was oxidized potentiodynamically. This CO oxidation will be referred to as CO_b oxidation.

For surface X-ray diffraction scattering measurements (SXS), the X-ray cell was mounted at the center of a four-circle goniometer on beamline 7-2 at the Stanford Synchrotron Radiation Laboratory. The outer shell of the electrochemical cell was purged with either nitrogen or CO. The CO diffused through the thin polypropylene film trapping the electrolyte.

In all the experiments 0.5 M H_2SO_4 (ULTREX II, J. T. Baker Reagent) prepared with triply distilled water was used. All potentials are referenced to the reversible hydrogen electrode (RHE) in the same solution and at the same temperature (298 K). A circulating constant temperature bath (Fisher Isotemp Circulator) maintained the temperatures of the solutions within ±0.5 K. A Pine Instruments Bipotentiostat (Model AFRDE 4; potential response 0.5 V/ms) was used for all the experiments. Pure (5N8) CO, CO/H_2, CO/Ar, and CO_2 gasses were purchased from Matheson.

RESULTS AND DISCUSSION

Carbon monoxide oxidation on low index platinum single crystals

Pt(111). The base voltammogram of Pt(111) disk electrode in 0.5 mol dm^{-3} H_2SO_4, onto which are superimposed the stripping of CO_{ads} in argon and oxidation of 100 % CO_b dissolved in the electrolyte is shown in Fig. 3. One should keep in mind that CO_b oxidation proceeds through the formation of CO_{ads} on the platinum surface. The interpretation of the base voltammogram of Pt(111) in sulfuric acid solution has been extensively discussed in the literature.[13] The potential region of hydrogen underpotential deposition, $\approx 0.07 < E < 0.3$ V is clearly separated from the potential region for adsorption/desorption of bisulfate anions, $\approx 0.3 < E < 0.5$ V. At a more positive potential, a small peak can be observed between the potentials 0.6 and 0.7 V, which corresponds to OH_{ads} formation, according to Eq. (3). Figure 3 shows that upon sweeping the potential positively from 0.05 V, the onset of CO_{ads} oxidation commences at ≈ 0.3 V. In the potential region between ≈ 0.3 and 0.6 V a small amount of CO_{ads} was oxidized (less than 20 % based on a full mono-layer of CO_{ads}, for more details see Ref. 14). It is impossible to oxidize more than 20 % of the CO_{ads} even by holding the potential in this region. This potential region is known as the preoxidation wave. Above 0.6 V, the stripping of CO_{ads} is characterized by two sharp peaks, a lesser peak at *ca*. 0.68 V and the major peak at ≈ 0.75 V. The oxidation of CO_{ads} above 0.6 V could be connected with OH_{ads} formation on Pt(111), which starts at the same potential. Electrooxidation of the gaseous CO dissolved in the bulk of the solution (CO_b), Fig. 3, starts at a potential of ≈ 0.3 V, but with a higher rate at ≈ 0.6 V. A sharp increase of CO_b oxidation is evident when the potential is more positive than 0.9 V.

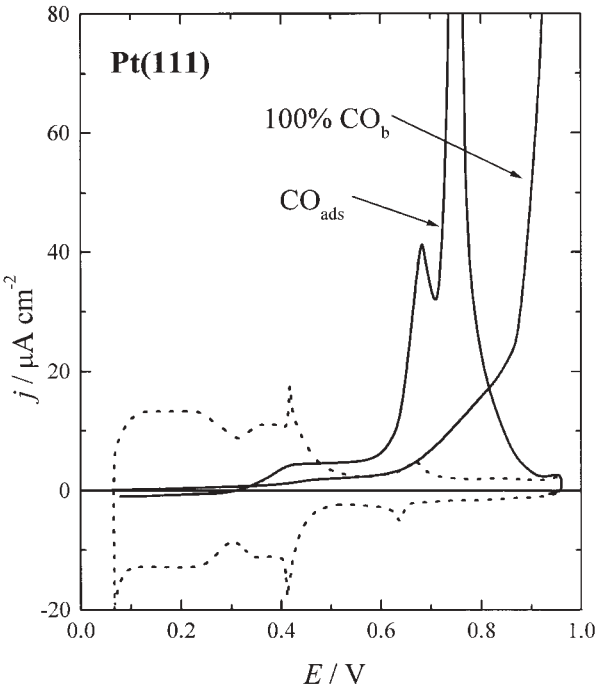

Fig. 3. Base voltammogram (50 mV/s) of a Pt(111) in 0.5 M H_2SO_4 onto which are superimposed the stripping voltammogram (20 mV/s) of CO_{ads} in an argon purged electrolyte and the potentiodynamic (20 mV/s) oxidation of 100 % CO_b.

Pt(100). The base voltammogram of Pt(100) in 0.5 mol dm^{-3} H_2SO_4, together with the oxidations of CO_{ads} and CO_b, are shown in Fig. 4. The characteristic features of the voltammogram of an ordered Pt(100) surface in sulfuric acid solution are two delineated peaks at 0.3 and 0.4 V, which mainly correspond to the coupled processes of hydrogen adsorption and bisulfate anion desorption on the (100) terrace sites and the (100)×(111) step sites, respectively.[15] The potential region of H_{upd} is followed, first by the revesible adsorption of OH_{ads} in the potential range $\approx 0.7 < E < 0.85$ V, and then by the irreversible formation of platinum oxide at potentials more positive than 0.9 V. The stripping voltammetry of CO_{ads} shows that, upon sweeping the potential positively from 0.05 V, the onset of oxidation commences at ≈ 0.3 V. Similar to the Pt(111) surface, before detectable OH_{ads} formation occurs, some oxidation of CO_{ads} could be seen from the preoxidation wave in the potential region of $0.3 < E < 0.65$ V. Above 0.75 V, the CO_{ads} stripping voltammogram is characterized by a sharp peak centered at 0.77 V. The potentiodynamic oxidation of CO_b is characterized by a huge preoxidation wave in the potential region between 0.32 and 0.97 V, with a maximum rate at ≈ 0.8 V. After that the current decreases and at potentials more positive than 0.97 V, the current sharply increases reaching a limiting diffusion current (not shown in the figure).

Pt(110). A characteristic of Pt(110) disk electrode is that, depending on the heat preparation treatment, it is possible to produce two different reconstructions. The 1×1 reconstruction was produced by rapid gas phase quenching (in argon–3 % hydrogen), and the 1×2 or missing row reconstruction was produced by slow cooling of the flame

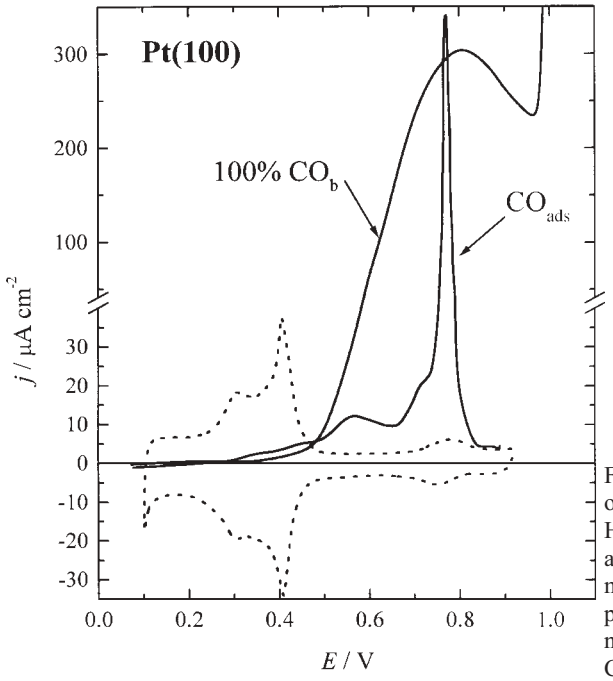

Fig. 4. Base voltammogram (50 mV/s) of Pt(100) disk electrode in 0.5 M H_2SO_4 rotating at 2500 rpm, onto which are superimposed the stripping voltammogram (20 mV/s) of CO_{ads} in argon purged electrolyte and the potentiodynamic (20 mV/s) oxidation of 100 % CO_b.

annealed crystal.[16] The base voltammogram of the Pt(110)×(1×1) and Pt(110)×(1×2) reconstructions in 0.5 mol dm^{-3} H_2SO_4, together with the oxidation of CO_{ads} and CO_b are shown in Figs. 5 and 6, respectively. The voltammetric features include reversible hydrogen adsorption/desorption peaks in the potential range of 0.05–0.35 V, (probably overlapped with bisulfate adsorption/desorption), and hysteretic peaks associated with oxide formation and reduction at more positive potentials. Significant differences in the Pt(110)–(1×2) voltammogram from the (1×1) one are: a broader hydrogen peak at *ca.* 0.1 V, a greater fraction of the total charge appearing in the potential region $\approx 0.15 < E <$ 0.3 V, and broader features in the oxide formation/reduction region. These differences are produced by the openness of the missing row structure. A close inspection of the voltammograms in Fig. 6 indicates that on sweeping the potential of Pt(110)–(1×2) to values more positive than ≈ 0.4 V some additional adsorption occurs, probably in the form of adsorbed hydroxyl adspecies, OH_{ads}.[16] The oxidation of carbon monoxide on the same structure with different reconstructions is surprisingly different. Oxidation of CO_{ads} and CO_b on Pt(110)–(1×1) are completely suppressed at potentials below 0.65 V and 0.86 V, respectively. CO_{ads} proceeds through a sharp peak in the potential region $0.65 < E < 0.75$ V, while CO_b oxidation starts at potentials more positive than 0.8 V, reaching the limiting diffusion current density, as shown in Fig. 5. On the contrary, on Pt(110)–(1×2), oxidation of a CO_{ads} starts at a potential of 0.3 V followed by the complete oxidation of the CO_{ads} adlayer through a broad peak in the potential region of $0.6 < E < 0.8$ V, Fig. 6. The onset of CO_b oxidation begins as early as *ca.* 0.45 V, appearing

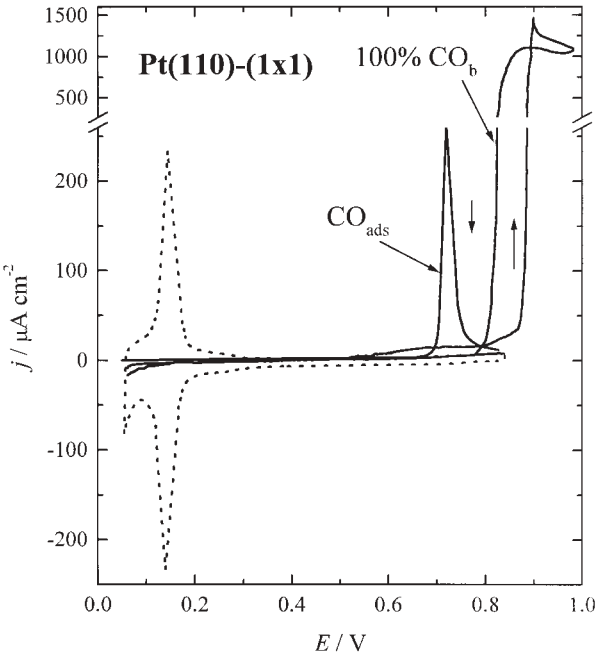

Fig. 5. Base voltammogram (50 mV/s) of Pt(110)–(1×1) disk electrode in 0.5 M H_2SO_4 rotating at 2500 rpm, onto which are superimposed the stripping voltammogram (20 mV/s) of CO_{ads} in argon purged electrolyte and the potentiodynamic (20 mV/s) oxidation of 100 % CO_b.

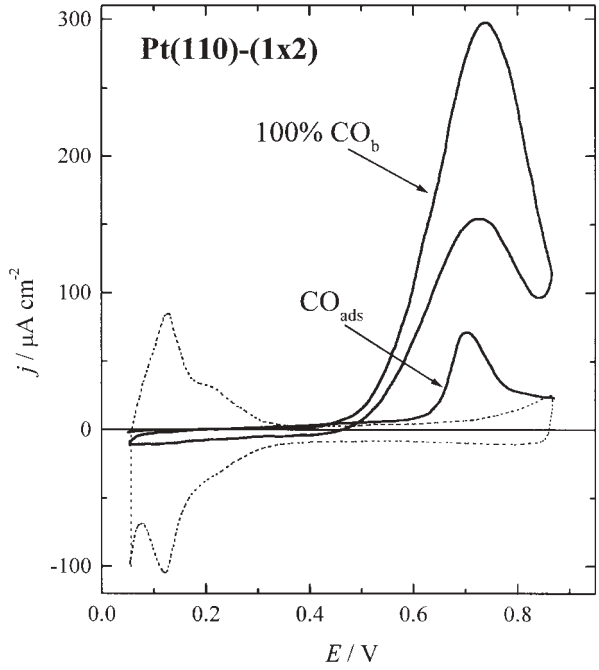

Fig. 6. Base voltammogram (50 mV/s) of Pt(110)–(1×2) disk electrode in 0.5 M H_2SO_4 rotating at 2500 rpm, onto which are superimposed the stripping voltammogram (20 mV/s) of CO_{ads} in argon purged electrolyte and the potentiodynamic (20 mV/s) oxidation of 100 % CO_b.

as a preoxidation wave in the potentiodynamic curves, Fig. 6, followed by a sharp increase of the current density at potentials higher than 0.8 V (not shown in the Figure).

Nature of CO_{ads} and the mechanism of CO oxidation on platinum surfaces

The results presented in the previous section indicate that the key to resolve the mechanism of the CO oxidation reaction on platinum electrodes lies in the state of CO_{ads}. For this reason the state of CO_{ads} was investigated by means of SXS (surface X-ray scattering diffraction measurements). In SXS it is typical to identify changes in the surface/interfacial structure by monitoring the intensity distribution of scattering in reciprocal space, and comparing the intensity distribution with that calculated for an atomic model. A precise description of the Pt surface structure at the Pt–CO_{ads} electrochemical interface can be obtained by measuring both the specular and nonspecular crystal truncation rods (CTRs), since H_{upd}, CO_{ads} and OH_{ads} are relatively weak scatterers making a negligible contribution to the Pt CTRs.[17] In this case, the CTRs yield information about the position of Pt surface atoms relative to the bulk position (commonly referred to as surface relaxation) as the electrode potential is changed and the coverage by adsorbates changes. The potential dependence of the relaxation of a Pt(111) surface induced by H_{upd} and/or CO_{ads} at 0.05 V is represented by the results in Fig. 7. In a solution free of CO, in the H_{upd} region, the top platinum layer expands, compared with the potential of minimum expansion (pme ≈ 0.7 V), by *ca.*

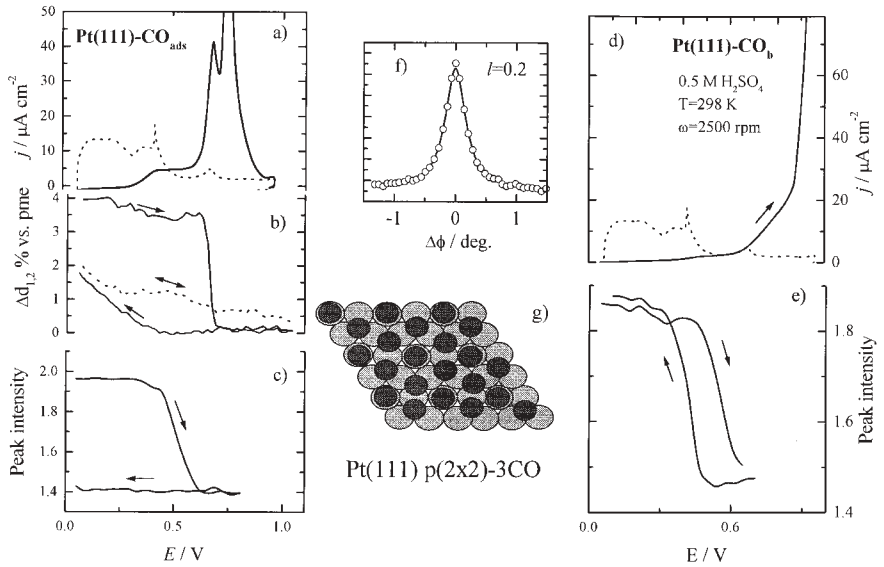

Fig. 7. a) (—) CO stripping and (---) base voltammogram of a Pt(111) disk electrode in 0.5 M H_2SO_4 rotating at 2500 rpm, in argon purged solution (taken from Fig. 2). b) SXS scattering intensity changes for (—) CO_{ads} covered and (---) free of CO_{ads} Pt(111)surfaces. c) Measured X-ray intensity (intensity of peak maximum from Fig. 7f) at (1/2, 1/2, 0.2) as a function of electrode potential under the same condition as in a). d) (—) potentidynamic oxidation of 100 % CO_b and (---) base voltammogram of a Pt(111) disk electrode in 0.5 M H_2SO_4 rotating at 2500 rpm (taken from Fig. 2). e) Same as c. f) A rocking scan through the (1/2, 1/2, 0.2) positions. g) Ideal model for the p(2×2)–3CO structure.

$\Delta d_{1,2} \approx 2$ % (0.05 Å) of the lattice spacing away from the second layer when H_{upd} reaches its maximum coverage, Fig. 7b. Following the adsorption of CO at 0.05 V, the expansion is even larger 4 %. This expansion remains constant on purging the CO_b from solution with nitrogen. The difference in relaxation of the Pt(111) surface covered with H_{upd} and CO_{ads} probably arises from the difference in the adsorbate–metal binding, the Pt(111)–CO_{ads} interaction being much stronger than the Pt(111)– H_{upd} interaction. Upon sweeping the potential positively from 0.05 V, the oxidation of CO_{ads} in the potential region of $0.3 < E < 0.6$ V is mirrored by a small contraction of the Pt surface layer, as shown in Fig. 7a and b. Above *ca*. 0.6 V, the top layer expansion is reduced significantly, contracting above 0.7 V to the same nearly unrelaxed state which the Pt(111) surface has without CO_{ads}. It is important to note that the most significant change in the surface relaxation is associated with the removal of ≈ 20 % CO_{ads} in the preoxidation region. Direct information regarding the CO_{ads} structure was obtained by searching the surface plane of reciprocal space for diffraction peaks characteristic of ordered adlayer structures. While holding the potential at 0.05 V and with continuous supply of CO_b to the X-ray outer cell, Fig 7e, a diffraction pattern, Fig. 7f, consistent with p(2×2) compressed symmetry was observed. The derived structural model is shown schematically in Fig. 7g, which consists of three CO_b molecules per p(2×2) unit cell. Once formed, the structure was stable even after the CO in outer cell had been replaced by nitrogen, Fig. 7b, confirming that CO is indeed irreversibly adsorbed on the platinum surfaces.

Having established the presence of the p(2×2)-3CO adlayer at 0.05 V, following the nitrogen purging of the CO_b, the scattering (peak) intensity at (1/2, 1/2, 0.2) was monitored as the electrode potential was swept positively. Figure 7c shows that potential range of stability of the p(2×2)-3CO phase is strongly affected by the oxidation of CO_{ads} in the preoxidation region. Clearly, the close correlation between the changes in the scattering intensity and the coverage by CO_{ads} (assessed from stripping voltammetry) suggest that the p(2×2)-3CO structure is present only in the potential range where the CO_{ads} coverage is higher than ≈ 0.8. Upon reversal of the electrode potential at *ca*. 0.6 V, the p(2×2)-3CO structures were unable to reform, confirming that this structure is governed by high CO_{ads} coverage and probably by high CO_{ads}–CO_{ads} lateral interactions (compression of CO_{ads} adlayer onto the surfaces). This supposition was tested by monitoring the peak intensity at the (1/2, 1/2, 0.2) position as the potential was changed, but this time with a constant overpressure of CO_b in the X-ray outer cell, Fig. 7e. These experiments revealed a reversible loss and reformation of the p(2×2)-3CO structure when sweeping the potential below ≈ 0.25 V.

In separate experiments, the CO_{ads} coverage was investigated by means of "hydrogen magnifier" experiments. Figure 8 shows the stripping voltammetry of CO_{ads} onto which are superimposed the linear sweep voltammetry curves of Pt(111) covered by adsorbed CO in H_2 saturated solution and the lienar sweep voltammetry curves of the oxidation of H_2/2 % CO gas mixtures. The polarization curve for the hydrogen oxidation reaction on a Pt(111) surface covered with the saturation coverage of CO_{ads} shows that after removing *ca*. 15 % of the CO_{ads} in the preoxidation region, rate of the hydrogen oxidation reaction sharply increases reaching a diffusion limiting current

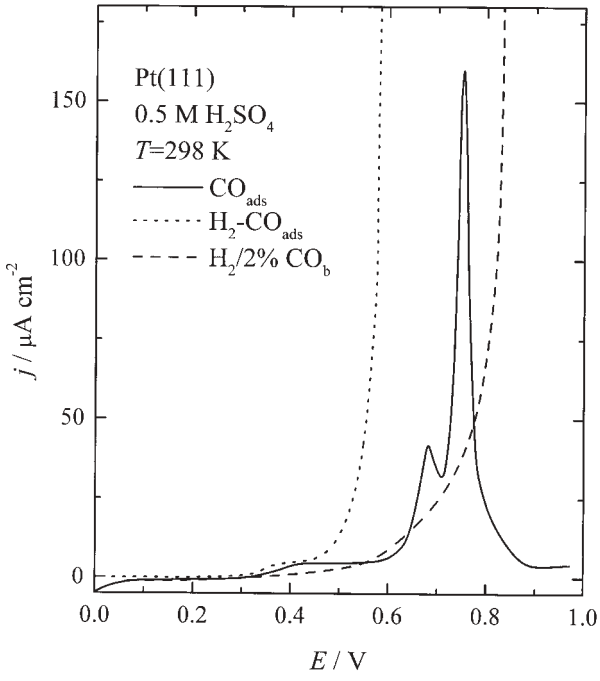

Fig. 8. (—) Stripping voltammogram (20 mV/s) of CO_{ads} in argon purged electrolyte of Pt(111) in 0.5 M H_2SO_4, (···) the potentiodynamic (20 mV/s) oxidation of pure hydrogen on CO_{ads} covered Pt(111), and (---) the potentiodynamic (20 mV/s) oxidation of a hydrogen–2 % CO_b mixture.

density at 0.6 V. On the contrary, the oxidation of hydrogen with 2 % of CO in the mixture is shifted positively by more than 0.3 V.

From all the presented data it is possible to analyze the state of CO_{ads} on the Pt(*hkl*) surfaces and propose a mechanism of CO oxidation. At maximum CO_{ads} coverage the energy of adsorption is strongly decreased due to lateral CO_{ads}–CO_{ads} interactions. Under UHV (ultra high vacuum) conditions, the energy of adsorption is decreased from 140 kJ mol^{-1} at zero coverage to ≈ 40 kJ mol^{-1} at maximum coverage.[18] The decrease of the energy of adsorption is pronounced when the CO_{ads} coverage is higher than 0.8. This means that at high coverage the CO_{ads} is weakly bonded onto the surface ($CO_{ads,w}$). As the level of coverage decreases below 0.8 then the energy of adsorption increases and the CO_{ads} becomes strongly adsorbed. ($CO_{ads,s}$). Hence, the preoxidation wave could be connected with the oxidation of weakly adsorbed CO_{ads}. The CO oxidation in the preoxidation region is structural sensitive, with the activity increasing in the order: Pt(110)–(1×1) < Pt(111) < Pt(110)–(1×2) < Pt(100). This difference in kinetics could be attributed to the competitive adsorption between water, anions from the supporting electrolytes and CO, as well as to differences in the energy of adsorption on the different crystal faces. Studies of CO_{ads} oxidation under UHV showed that the oxidative removal of CO_{ads} occurs between oxygen chemisorbed preferentially on the step sites and CO_{ads} on the terrace sites.[33] This concept can be extended to the solid-liquid interface, as such a mechanism could explain, at least in part, the structure sensitive co-adsorption of CO_{ads}, OH_{ads} and bisulfate anions. The details of the coa-

dsorption are, however, by no means unambiguous. Nevertheless, it is essential to point out that Pt(110)–(1×1) exposes only first-layer atoms to the reactants (CO_{ads} and OH_{ads}) and/or spectators (bisulfate anions). The formation of a saturated layer of CO_{ads} on this surface can lead to the complete occupation of the top rows of Pt atoms by $CO_{ads,w}$, resulting in a low surface coverage by OH_{ads} and, consequently, in a low rate of reaction (1). In contrast, the Pt(110)–(1×2) surface may expose second and third layer atoms to the reactants and spectators, and these species may occupy both the top rows of platinum atoms (step sites) as well as the atoms in the missing rows. Note that the missing rows in the (110)–(1×2) structure create "valleys" between the (110) rows consisting of the three-atom-wide(111) terrace. The geometry of the adsorption sites in the valleys are like those in the flat (111) surface or the (111) terraces of stepped surfaces. The sites on the (110) rows of atoms are common to the step sites on many types of step-terrace structures. Thus, the (110)–(1×2) has a mixture of sites for the coadsorption of both $CO_{ads,w}$ and OH_{ads} which are absent in the the (110)–(1×1) structure. Considering that it can safely be generalized that even "flat" low index metal surfaces may well contain a certain number of crystallographic defects, it is reasonable to suggest that the rate of CO oxidation in the preoxidation region on Pt(100) and Pt(111) depends on the density of mono-atomic steps capable of adsorbing OH_{ads}. Recently it has been shown that a Pt(100) surface prepared by the flame annealing method is an intrinsically defected structure.[20] Therefore, the preoxidation wave on Pt(100) can be attributed to the unique catalytic property of step/defect sites to activate adsorption of OH_{ads} species which can react with $CO_{ads,w}$ on the flat terrace sites. Based on the fact that a Pt(111) surface has less defects than both the Pt(110)–(1×2) and Pt(100) surface, it is reasonable to propose that, under identical conditions, there is insufficient nucleation of OH_{ads} on Pt(111) for the oxidation of $CO_{ads,w}$, to proceed in sulfuric acid solution, when CO is present in solution. Consequently, Pt(111) is less active for CO_b oxidation in the preoxidation region than either Pt(110)–(1×2) or Pt(100).

Hence, in the preoxidation region, the mechanism of CO_{ads} oxidation can be given by the following mechanisms

$$H_2O + CO + 2Pt \rightleftharpoons Pt - CO_{ads,w} + Pt - OH_{ads} + H^+ + e^- \quad (4a)$$

$$Pt - CO_{ads,w} + Pt - OH_{ads} \rightarrow Pt - [CO - OH]_{ads} + Pt \quad (4b)$$

$$Pt - [CO - OH]_{ads} \rightleftharpoons CO_2 + H^+ + Pt + e^- \quad (4c)$$

or

$$H_2O + CO + 2Pt \rightleftharpoons Pt - CO_{ads,w} + Pt - OH_{ads} + H^+ + e^- \quad (5a)$$

$$Pt - CO_{ads,w} + Pt - OH_{ads} \rightarrow CO_2 + H^+ + 2Pt + e^- \quad (5b)$$

In the mechanism given by the sequence 4a-c, the rate determining step is the heterogeneous chemical reaction between OH_{ads} formed at step sites and adjancent $CO_{ads,w}$ at the terrace sites. In the mechanism given by the sequence 5a-b the rate deter-

mining step is the heterogeneous electrochemical reaction. It is imposible to say which of these two mechanisms is more probable.

After removing the $CO_{ads,w}$, at potentials higher than ≈ 0.6 V, nucleation of OH_{ads} occurs at the terrace sites, which allows attack on the edge of $CO_{ads,s}$ islands and complete oxidation of CO_{ads} from the surfaces. The mechanism is probably similar to that given by 5a-b.

The oxidation of CO_b is somewhat different because the repopulation of $CO_{ads,w}$ in the preoxidation region by CO adsorption from solution allows constant oxidation of $CO_{ads,w}$ by OH_{ads} from the step sites. At more positive potentials, where OH_{ads} are nucleated at terrace sites at a higher rate, $CO_{ads,w}$ cannot be repopulated at the same rate and so the reaction rate decreases. The maximum rate, limiting diffusion current density, of CO_b oxidation is reached at potentials more positive than ≈ 0.9 V when platinum starts to form oxides (Pt – OH) on the surface. The mechanism of this could be given by:

$$H_2O + CO + 2Pt \rightleftarrows Pt - CO_{ads} + Pt - OH + H^+ + e^- \quad (6a)$$

$$Pt - CO_{ads,s} + Pt - OH \rightarrow CO_2 + H^+ + 2Pt + e^- \quad (6b)$$

For application in fuel cells it is important to free of CO_{ads} the platinum atoms on which hydrogen oxidation reaction can occur. The mechanism of hydrogen oxidation in H_2/CO mixtures on platinum can be given by the following sequences:

$$CO_b + Pt \xrightarrow{k_{ads}(CO)} Pt - CO_{ads} \quad (7a)$$

$$Pt + H_2O \rightleftarrows Pt - OH_{ads} + H^+ + e^- \quad (7b)$$

$$Pt - CO_{ads} + Pt - OH_{ads} \xrightarrow{k_{ox}(CO)} CO_2 + H^+ + 2Pt + e^- \quad (7c)$$

$$2Pt + H_2 \rightarrow 2Pt - 2H_{ads} \quad (7d)$$

$$2Pt - 2H_{ads} \rightarrow 2Pt + 2H^+ + 2e^- \quad (7e)$$

The H_2 oxidation reaction occurs on the free sites liberated during the time between CO_{ads} oxidative removal, Eq (7c), and CO readsorption from solution, Eq (7a). The rate constant of CO_b readsorption is much higher than the rate constant for CO_{ads} oxidation, and practically only an infinitely small number of platinum sites could be liberated for H_2 oxidation. The hydrogen oxidation reaction reaches maximum at the same potential where CO is oxidized by Pt – OH (coverage with CO_{ads} in that potential region tends to zero). According to this, it is necessary to provide a supply of OH species to adjunct platinum atoms covered by CO_{ads} by some other metal which does not adsorb CO. This can be done by alloying the platinum with some other metals, which will be treated in the second part of this paper.

И З В О Д

ЕЛЕКТРОХЕМИЈСКА ОКСИДАЦИЈА УГЉЕН-МОНОКСИДА: ОД МОНОКРИСТАЛА ПЛАТИНЕ ДО КАТАЛИЗАТОРА ЗА НИСКОТЕМПЕРАТУРНЕ ГОРИВНЕ ГАЛВАНСКЕ СПРЕГОВЕ. I ДЕО: ОКСИДАЦИЈА УГЉЕН–МОНОКСИДА НА НИСКОИНДЕКСНИМ МОНОКРИСТАЛИМА ПЛАТИНЕ

БРАНИМИР Н. ГРГУР[1], НЕНАД М. МАРКОВИЋ[2], CHRISS C. LUCAS[3] и PHILIP N. ROSS JR.[2]

[1]Технолошко-металуршки факултет, Универзитет у Београду, Карнегијева 4, 11001 Београд, Југославија, [2]Lawrence Berkeley National Laboratory, 1 Cyclotron Road, MS 2-100, Berkeley, CA 94720, USA, и [3]Oliver Lodge Laboratory, Department of Physics, University of Liverpool, Liverpool L69 7ZE, UK

Коришћењем технике ротирајуће диск електроде и *in-situ* технике површинске дифракције X-зрака, испитивана је реакција електрохемијске оксидације угљен-моноксида и природа адсорбованог CO на монокристалима платине ниских индекса оријентације, Pt(111), Pt(100) и две реконструкције Pt(110). Дискутован је механизам оксидације CO на основу установљеног постојања два енергетска стања адсорбованог угљен-моноксида, слабо везаног стања при нижим потенцијалима и чврсто везаног стања при вишим потенцијалима. Такође је дискутован механизам оксидације смеша водоника са угљен-моноксидом.

(Примљено 16. јула 2001)

REFERENCES

1. R. Kumar, S. Ahmed, Proc. *First Internat. Symp. on New Materials for Fuel Cell Systems,* O. Savadogo P. Roberge, T. N. Verziroglu, Eds., Ecole Polytechnique de Montreal, Montreal, 1995, pp. 243–238
2. G. Blyholder, *J. Phys. Chem.* **68** (1964) 2772
3. S. Gilman, *J. Phys. Chem.* **68** (1964) 70
4. J. Sobkowski, A. Czerwinski, *J. Electroanal. Chem.* **91** (1978) 47
5. V. E. Kazarinov, V. N. Andreev, A. V. Shlepakov, *Electrochim. Acta* **34** (1989) 905
6. M. Watanabe, S. Mooto, *J. Electroanal. Chem.* **60** (1975) 267
7. H. A. Gasteiger, N. M. Marković, P. N. Ross, *J. Phys. Chem.* **99** (1995) 8290; H. A. Gasteiger, N. M. Marković, P. N. Ross, *J. Phys. Chem.* **99** (1995) 16757
8. H. A. Gasteiger, N. M. Marković, P. N. Ross, *J. Phys. Chem.* **99** (1995) 8945
9. M. Iwase, S. Kawatsu, Proc. *First Internat. Symp: Proton Conducting Membrane Fuel Cells I*, Vol. 95–26, The Electrochem. Soc. INC. Penington, NJ., 1995
10. N. M. Marković, B. N. Grgur, P. N. Ross, *J. Phys. Chem. B.* **101** (1997) 5405
11. N. M. Marković, A. Widelov, P. N. Ross, O. Montero, I. Brown, *Cat. Lett.* **43** (1997) 161
12. T. J. Scmidt, H. A. Gasteiger, G. D. Stab, P. M. Urban, D. M. Kolb, R. J. Behm, *J. Electrochem. Soc.* **145** (1998) 2354
13. J. Clavilier, A. Rodes, K. El Achi, M. A. Zamakhchari, *J. Chim. Phys.* **88** (1991) 1291
14. N. M. Marković, B. N. Grgur, C. A. Lucas, P. N. Ross, *J. Phys. Chem. B.* **3** (1999) 487
15. N. M. Marković, N. S. Marinkvic, R. R. Aldaz, *J. Electroanal. Chem.* **214** (1988) 309
16. N. M. Marković, B. N. Grgur, C. A. Lucas, P. N. Ross, *Surf. Sci.* **384**(1997) 805
17. M. F. Toney, O. R. Merloy, in *In-situ Studies of Electrochemical Interfaces,* H. O. Abruna, Ed., VCH, Berlin, 1991
18. R. Masel, *Principles of Adsorption and Reaction on Solid Surfaces*, Wiley, New York, 1996
19. J. Xu, J. T. Yates, *J. Chem. Phys.* **99** (1993) 725
20. N. M. Marković, B. N. Grgur, C. A. Lucas, P. N. Ross, *Electrochim. Acta.* **6 – 7** (1998) 10009.